HHS Public Access

Author manuscript

Immunobiology. Author manuscript; available in PMC 2022 May 01.

Published in final edited form as:

Immunobiology. 2021 May ; 226(3): 152089. doi:10.1016/j.imbio.2021.152089.

Full Length RAG2 Expression Enhances the DNA Damage Response in Pre-B Cells

Jennifer N. Byrum, **Walker E. Hoolehan**, **Destiny A. Simpson**, **William Rodgers**, **Karla K. Rodgers***

Department of Biochemistry and Molecular Biology, University of Oklahoma Health Sciences Center, Oklahoma City

Abstract

V(D)J recombination by the RAG1 and RAG2 protein complex in developing lymphocytes includes DNA double strand break (DSB) intermediates. RAG2 undergoes export from the nucleus and enrichment at the centrosome minutes following production of DSBs by genotoxic stress, suggesting that RAG2 participates in cellular responses to DSBs such as those generated during V(D)J recombination. To determine the effect of RAG2 expression on cell viability following DSB generation, we measured pre-B cells that expressed either full length (FL) wild-type RAG2, or a T490A mutant of RAG2 that has increased stability and fails to undergo nuclear export following generation of DSBs. Each RAG2 construct was labeled with GFP at the N-terminus. Compared to the T490A mutant, cells expressing FL RAG2 exhibited elevated apoptosis by 24 hours following irradiation, and this coincided with a greater amount of Caspase 3 cleavage measured in cell lysates. Pre-B cells expressing either RAG2 protein exhibited similar increases in phospho-p53 levels following irradiation. Interestingly, FL RAG2-expressing cells exhibited elevated division relative to the T490A clone beginning ~24 hours following irradiation, as well as an increased percentage of cells proceeding through mitosis, suggesting an improved rate of recovery following the initial burst in apoptosis. Altogether, these data show that FL RAG2, but not its stable nuclear export-defective T490A mutant, participates in pre-B cell decisions between apoptosis versus DNA repair and cell cycle progression following DNA damage.

Keywords

V(D)J recombination; RAG1; RAG2; DNA repair; genotoxic stress; DNA damage response; apoptosis; cell cycle; pre-B cells

Introduction

B and T cells in the human adaptive immune system collectively express a vast array of antigen receptors with differing binding specificities to foreign antigens (1,2). This diverse

*To whom correspondence should be addressed: karla-rodgers@ouhsc.edu, Tel: +1-405-271-2227x61248.

repertoire of antigen receptors, immunoglobulins (Ig) in B cells and T cell receptors (TCR) in T cells, underlies the strength of the immune systems in all jawed vertebrates. V(D)J recombination assembles functional antigen receptor genes in the appropriate cell lineage from pools of component gene segments, termed V, D, and J (1,2). Eligible gene segments for V(D)J recombination are flanked by a conserved recombination signal sequence (RSS). The V(D)J recombinase, consisting of RAG1 and RAG2, catalyzes the initial DNA double strand breaks (DSBs) at the border of selected gene segments and their flanking RSS (3,4). Subsequent to RAG-mediated DNA cleavage activity, the nonhomologous DNA end joining (NHEJ) pathway functions to join cleaved gene segments to create the exon encoding for the antigen recognition region of the receptors (5,6).

For expression of the B cell receptor, V(D)J recombination must successfully rearrange the Ig heavy chain locus (IgH) through a D to J and the V to D-J joining, as well as at the Ig light chain loci (Igκ Igλ) through a V-J joining (1,2). This requires multiple cycles of RAG-mediated cleavage reactions and NHEJ to produce in-frame rearrangements at both heavy and light chain loci. An analogous situation occurs at TCR loci in developing thymocytes.

V(D)J recombination activity leads to activation of a DNA damage response (DDR) system spearheaded by ATM and DNA-PKcs, which leads to cell cycle arrest in G1 (7,8). Activation of these kinases leads to formation of γH2AX foci at the RAG-mediated DNA breaks, and phosphorylation of 53BP1 recruited to the breaks. ATM also functions to stabilize the RAG-generated DNA ends (9,10), while DNA-PKcs plays a well-known role in NHEJ and coding end repair (5,6). Overall, RAG-mediated DNA DSBs yield effects similar to cell responses to DNA damage produced by exogenous genotoxic agents (7). Besides induction of DDR, RAG-mediated DNA breaks at antigen receptor loci drives transcriptional reprogramming that promotes progression of B cell development (11). Interestingly, ionizing radiation (IR) induces a similar transcriptional reprogramming response in developing murine B cells (11,12).

The programmed RAG-mediated DNA DSBs in V(D)J recombination are essential for continued B and T cell development, as defects in RAG expression or activity results in immunodeficiency diseases (13). Nonetheless, DNA DSBs represent the most deleterious form of DNA damage and incorrect targeting of RAG cleavage can lead to chromosomal aberrations and genomic instability (7,8,14). Further, error in the repair of RAG-mediated DNA ends are significantly increased in cells containing excess DNA DSBs that are induced by exogenous sources, such as IR or chemotherapeutic drugs (7).

V(D)J recombination is normally limited to G1 under normal conditions due to degradation of RAG2 at G1/S, which is dependent on RAG2 residue T490 (15).

However, additional regulation of RAG activity is required during conditions of genotoxic stress to mitigate errant V(D)J recombination. For example, treatment of pre-B cells with DNA damaging drugs was shown to downregulate RAG1 and RAG2 mRNA, degrade the RAG1 protein, and accordingly reduce V(D)J recombination activity within 1 hour (16). Despite downregulation of its mRNA, RAG2 remains stable for at least 24 hours after introduction of DNA damaging agents (17). Further, we previously determined that a

significant fraction of nuclear RAG2 is exported to the cytosol in an exportin-1 and ATM-dependent manner following ionizing radiation (IR), where a measurable fraction of cytosolic RAG2 specifically localizes to the centrosome (18). These effects are reversed by 4 hours post-IR following repair of the majority of DNA breaks. The RAG2 T490A mutant, which is not subjected to cell cycle dependent degradation, blocks the ATM-dependent nuclear export of RAG2 upon genotoxic stress (18). Interestingly, this mutant showed increased nuclear localization even in the absence of genotoxic stress, which is consistent with its increased co-localization with open chromatin and concomitant decrease in diffusion rate (19). Given these differential effects, we tested how pre-B cells expressing FL versus T490A RAG2 compared regarding cell survival and recovery following genotoxic stress.

Materials and Methods

Cell culture and generation of DSBs

v-abl RAG2$^{-/-}$ pro-B cells (63-12) were cultured in media containing RPMI with glutamine, 10% FBS, 1% non-essential amino acids (GE Healthcare Life Sciences-Marlborough, MA), 1% antimycotic antibiotic (Corning-Corning, NY), and 0.1% beta-mercaptoethanol (Sigma-Aldrich-St. Louis, MO). Cells were cultured at 37° C in the presence of 1 mg/mL of G418. GFP-fusion proteins were expressed as previously described (18), and for this study included the full length RAG2 protein (FL) and the RAG2 point mutant T490A, each with GFP fused at the N-terminus. The clones were enriched every 4–6 weeks using flow cytometry, selecting cells that had detectable GFP fluorescence, and as a negative control gating on cells that were mock transfected. Relative expression levels of FL and T490A was assessed by western blots using stable clones with and without induction of endogenously expressed RAG1 (Supplemental Materials and Methods, Supplemental Figure 1). V(D)J recombination activity at the Igκ loci was assessed in pro-B cells stably expressing FL and T490A by PCR of isolated genomic DNA (Supplemental Figure 2). In experiments requiring expression of RAG1, cells were grown overnight in 1.5 mg/mL G418. To generate DSBs, cells were irradiated with 4Gy using a Cs^{137} gamma irradiator (Gammacell-40 exactor), at a dose of 1.1 Gy/min. Cells were immediately transferred post-IR to 37° C and maintained for the indicated times.

Fluorescence labeling and analysis

For immunostaining, cells were seeded onto coverslips (15 mm #1.5, Corning-Tewksbury, MA) at a density of 10^6 using poly-L-lysine (Sigma-Aldrich), fixed in 4% paraformaldehyde (Sigma-Aldrich) at room temperature for 30 minutes, and permeabilized using 0.1% Triton X-100 (Sigma-Aldrich) in PBS containing 10 mM glycine (PBS-glycine). Samples were stained with antibody to γ-tubulin (GTU-88, Sigma-Aldrich), then secondary anti-Ig labeled with DyLight 594 (Vector Labs, Burlingame, CA), followed by DAPI for labeling of cell nuclei. Images were taken using a Nikon (Tokyo, Japan) Eclipse T*i* series microscope. Images were quantified using iVision (BioVision Technologies, Exton, PA). For centrosome analysis, cells immunostained with γ-tubulin were overlayed with DAPI stain to observe localization of each foci.

To measure apoptosis after DNA damage, cells were incubated with fluorochrome-conjugated Annexin V (eBioscience, San Diego, CA), followed by 7-AAD Viability Staining Solution, then analyzed by flow cytometry. For intracellular staining of samples for flow cytometry, cells were fixed and permeabilized in 70% ethanol for 30 minutes on ice, followed by staining with either Propidium Iodide (Abcam), or antibody to phosphorylated Histone H3 (Cell Signaling Technology, Danvers, MA) and secondary Cy3 anti-rabbit (Jackson ImmunoResearch, West Grove, PA). Data were analyzed using FlowJo, LLC. Software.

Western blot analysis

Cell lysates were separated by SDS-PAGE, 10% acrylamide, at a density of 10^5 cells per well, transferred onto PVDF (Millipore-Burlington, MA), and immunoblotted with one of the following primary antibodies: rabbit monoclonal anti-Cleaved Caspase-3 (Asp175/5A1E, Cell Signaling Technology, Danvers, MA), rabbit polyclonal anti-Phospho-p53 (Ser15, Cell Signaling Technology), or rabbit monoclonal anti-GAPDH (EPR16891, Abcam). Biotinylated anti-rabbit secondary antibody was used for all blotting assays, and ECL Prime (Sigma-Aldrich) was used for chemiluminescence detection and visualized with a BioRad Chemidoc MP gel imaging system.

Statistical Analysis

Statistical analysis was performed using Prism 8 (GraphPad Software, La Jolla, CA). Standard deviation (SD) was determined using the average of at least 3 trials. Two-tailed Student's *t*-test was used to determine statistical significance, where **, $p < 0.01$, and *, $p < 0.05$.

Results

Full length RAG2 increases apoptosis in pre-B cells following DNA damage.

To determine the effect of RAG2 expression on cell survival following formation of DSBs, $RAG2^{-/-}$ pre-B cells stably expressing GFP fused to FL RAG2 or T490A RAG2 (Supplemental Figure 1A) were exposed to 4 Gy IR, cultured for 24 hrs, and then fixed and stained with labeled Annexin V to detect apoptotic cells. Cells expressing GFP alone (not fused to RAG2) served as a control for properties specific to RAG2 expression. Labeling with Annexin V was measured by flow cytometry. In Figure 1A are representative data from a single trial, and the averaged data from three separate trials are plotted in Figure 1B. There was minimal staining by 7-AAD for all cell samples, indicating that the cells were intact and that Annexin V-staining was due to apoptotic, and not necrotic, cells (not shown). Altogether, these data show that expression of the labeled RAG2-FL increased the fraction of Annexin V-positive cells relative to that which occurred in the RAG2-T490A and GFP samples.

Notably, in unirradiated cells the FL sample showed a mixture of low and high GFP+ cells (Figure 1A; middle row, left panel), where the T490A and control GFP samples show primarily the high GFP+ population. In the 24 hr post-IR sample, (Figure 1A, right middle panel) the GFP signal for the FL sample shifted to a primarily high GFP+ population. The

shift to GFP+ cells is likely due to cell cycle arrest in G1 upon detection of DNA damage by the DDR system, where RAG2 FL is expressed at higher levels. In contrast, it has previously been shown that RAG2 T490A is expressed in S and G2 cell cycle phases (20), and thus does not show this change in expression level following DNA damage.

To better determine the properties of the IR-induced apoptosis in the RAG2-expressing cells, we measured caspase-3 cleavage by immunoblotting whole cell lysates at 2, 4, 24, and 48 hours post-IR. In Figure 2A is a representative immunoblot showing IR-induced cleaved caspase in both the FL and T490A samples, and in Figure 2B is the averaged data from separate trials. These data show both samples exhibited an increase in caspase-3 cleavage following exposure to IR, but both the rate and amount of increase in caspase 3 cleavage consistently trended greater for the FL- than the T490A-expressing cells. Accordingly, RAG2 FL-expressing cells exhibited, on average, a two-fold increase in caspase 3 cleavage by 8 hours post-IR, whereas the RAG2 T490A sample required 48 hrs to achieve this value (Figure 2B). Altogether, these data show that FL expression initially increased pre-B cell apoptosis post-IR relative to cells that expressed T490A.

Cell cycle checkpoint activation following DNA damage.

Upon DNA damage, cells undergo a p53-dependent checkpoint control to direct the cell to either cell cycle arrest and apoptosis, or DSB repair for continued propagation and survival (21). To show whether the separate apoptotic responses of FL- versus T490A-expressing cells following irradiation was related to differences in p53 activation, we measured activated p53 at separate time points up to 48 hr post-IR In this experiment, the activated p53 was measured by immunoblotting whole cell lysates with antibody specific to phospho-p53 at the indicated time points (Figure 2C). Both cell lines exhibited an increase in phospho-p53 content following irradiation, and the amount and rate of change was essentially equivalent for FL- and T490A-expressing pre-B cells, when averaged over n=3 trials (Figure 2D). Accordingly, the elevated apoptosis in FL-expressing cells following exposure to IR is not specific to higher levels of p53 activation.

Expression of full length RAG2 increases proliferation following irradiation.

Since cells that are not directed to apoptosis during checkpoint control are allowed to repair and proliferate, we asked whether either RAG2 construct affected pre-B cell proliferative responses following irradiation. Pre-B cells expressing either FL, T490A, or GFP control were labeled using a cell-permeable dye (Cell Tracker Orange) and measured by flow cytometry at 0-, 24-, and 48-hours post-IR. Gating on cells at the initial time point, we observed comparable proliferation at 24 hrs post-IR in cells that expressed either RAG2 protein relative to control cells that expressed GFP alone, as measured by the GFP peak value at the 24 hr timepoint (Figure 3A). We noted that the peak area at 24 hrs relative to 0 hrs is ~5–10% less for FL versus T490A or the GFP control (Figure 3A), which is consistent with the increased apoptosis for the FL sample at this timepoint (Figure 1). Interestingly, FL-expressing cells subsequently exhibited increased proliferation by 48 hrs post-IR than to cells that expressed T490A or the GFP control. For example, measuring the difference in peak GFP intensity values using the 24 and 48 hr time points showed the difference was over one-third greater for the FL sample compared to the T490A and GFP samples (Figure 3B).

Thus, following a slight lag in cell division of FL-expressing cells, the relatively rapid proliferation by 48 hrs suggest a more robust recovery for the remaining FL-expressing cells as compared to T490A-expressing and GFP control cells.

Progression through cell cycle phases for FL versus TA RAG2-expressing cells

We determined the proportion of cells in G1 versus S/G2 cell cycle phases in nonirradiated cells and in cells up to 48 hrs post-IR by PI staining (Figure 4A). The FL and control GFP samples showed an increase in G1 in the post-IR samples in the range of 3–8% as compared to the nonirradiated cells. Interestingly, as compared to FL and the GFP control samples, the cell cycle phase distribution of the T490A sample showed the lowest percentage of cells in G1 for both nonirradiated cells and for cells 24 and 48 hr post-IR (Figure 4A). The T490A mutation decreases the amount of degradation of RAG2 at the G1/S border (15), and its continued expression afterwards may affect the fraction of cells that occur in G1 relative to S/G2.

We next evaluated the effect of RAG2 expression on cell cycle progression by measuring phosphorylation of Ser10 and Ser28 of histone H3 at 24 hrs post-IR. H3 phosphorylation at Ser10 and Ser28 are markers of mitosis and is indicative of progression through the cell cycle from G1 into M (22). These data are consistent with the proliferation data in Fig. 3, showing that FL-expressing cells contained increased H3 phosphorylation content following irradiation, indicating that surviving FL-expressing cells are capable of progressing through the cell cycle (Figure 4B). Interestingly, expression of T490A was associated with low levels of H3 phosphorylation in irradiated cells, indicating decreased progression through mitosis as compared to FL-expressing cells.

We also measured mitotic cells based on the presence of duplicated centromeres (Fig. 4C). Scoring the number of cells with duplicated centrosomes, our findings again showed an elevated number of mitotic cells in FL-expressing cells at most time points following irradiation compared to cells that expressed either T490A or GFP (Figure 4D). Also, as in Fig. 4B, T490A shows a substantial decrease of cells in mitosis.

Overall, by two separate methods (Fig. 4B and Fig. 4D) T490A-expressing cells show decreased propensity to proceed into mitosis following IR, despite relatively elevated populations of cells in S/G2 as compared to FL and GFP control samples (Fig. 4A). Importantly, the data in Figure 4 are consistent with that in Figure 3 showing expression of FL, but not T490A, increases pre-B cell proliferation.

Discussion

V(D)J recombination catalyzes multiple rounds of DNA damage and repair during development of each B and T cell, which is requisite for lymphocyte development (3,4). However, since DNA double-strand breaks are the most deleterious form of DNA damage (21), it is important to determine how the cell responds to the RAG proteins. Here, we found distinctly different responses of FL- versus T490A-expressing pre-B cells to genotoxic stress. In this study, we generated genotoxic stress with a short burst of IR, and then monitored cellular responses, including apoptosis and cell proliferation, with time.

Following IR, the short term response (within 24 hrs post-IR) includes increased apoptosis for cells expressing FL RAG2 as compared to T490A or the GFP control samples (Fig. 5A). Following the initial increase in apoptosis, the remaining FL cell population shows an increased rate of recovery compared to either the T490A or the GFP control samples in a long term response (up to 72 hrs post-IR; Fig. 5). Overall, our results in this study indicate that FL RAG2 can bolster DDR upon genotoxic stress in pre-B cells, and this may occur by more effective elimination of damaged cells within the first few hours following the occurrence of DNA damage.

Previous findings have indicated that RAG2 expression in developing B cells affects the maintenance of genomic stability. For example, in $p53^{-/-}$ mice, FL RAG2 was proposed to exhibit tumor suppressor activity, as truncated RAG2 lacking the entire non-core region led to an increase in the incidence of chromosomal translocations (23). This effect was attributed to increased stability in interactions of DNA ends for FL versus truncated RAG2, which promoted repair by the classical NHEJ factors. In a separate study, T490A RAG2 knock-in mice showed an increased incidence of B cell lymphomas, possibly due to decreased restriction of RAG activity to the G1 phase of the cell cycle and subsequent repair of DNA ends outside of G1 by alternative DNA DSB repair pathways (15). Along those lines, since the non-core region of RAG1 was shown to bind to Ku (24), it is feasible that the full length RAG proteins may facilitate rapid repair of DNA ends by efficiently directing the properly paired DNA ends to NHEJ factors.

Previous studies of the effect of DNA damage on RAG protein expression and stability indicates the RAG2 protein, in contrast to RAG1, remains stable after DNA damage, despite downregulation of its mRNA (17). The stabilization of RAG2 protein could be attributed to decreased cell egress into the S phase upon cell cycle arrest, implying that RAG2 is an inert bystander during DDR and DNA repair. However, our previous studies showed that following genotoxic stress, FL RAG2 exported from the nucleus in an ATM-dependent manner, where it enriched at the centrosome (18) (Fig. 5B). Consistent with these findings, we identified several centrosomal proteins that likely directly or indirectly associate with FL RAG2 in cells at 30 minutes post-IR, but not in untreated cells (Supl Fig. 3). Uncoupling of centrosome duplication from the cell cycle upon DNA damage would be deleterious to the cell (25), and multiple mechanisms may exist that ensure these central processes remain tightly coupled upon DNA damage. As shown previously, there is no evidence of centrosome localization upon DNA damage by the core only region of RAG2 (18), indicating that the non-core region of RAG is required (Supl Fig 4). We attempted to mutate the C-terminal nuclear localization signal of RAG2 to determine the effect of cytosolically-restricted RAG2 on the DDR; however, the NLS RAG2 mutant appeared to be show strong localization to a distinct area of the cytoplasm of unknown function, even in the absence of DNA damage (Supl Fig 5), thereby compromising interpretation of findings regarding cytoplasmic restriction of RAG2 on the extent of DDR. Potential function of FL RAG2 at the centrosome upon activation of DDR will require further study.

An alternate mechanism whereby RAG2 leads to increased DDR can be attributed to cellular responses to RAG-mediated DNA cleavage. For example, low levels of V(D)J recombination activity may yield sufficient DNA damage, which would result in a long-term consequence

on the relative strength of DDR and DNA repair systems. For example, natural killer (NK) cells that had previously expressed RAG proteins during their development showed a more robust DDR in the face of excess DNA damage versus NK cells that had not previously expressed the RAG proteins (26). This was attributed to a priming of the DDR system in the NK cells due to the history of RAG-mediated DNA damage. In our stable clones, we have detected RAG1 expression even in the absence of STI-571 (Supl Fig 1). We surmise that as the cell cycles through G1, low levels of RAG DNA cleavage activity occurs, resulting in a priming of the DDR system. Thus, for ~24 hrs following the generation of genotoxic stress, the DDR-primed cells will more efficiently initiate apoptosis of damaged cells. Following the initial phase of apoptosis, the remaining population of cells are likely more robust and the cell population is capable of faster recovery.

In our stable clones, the DDR in T490A RAG2-expressing cells is notably deficient. In particular, cell cycle progression was deficient in the T490A-expressing cells, with few, if any, cells progressing into mitosis several days following the generation of DNA damage (Fig. 4). Besides decoupling of the T490A mutant from cell cycle-dependent regulation, our previous studies showed that T490A RAG2 exhibited significantly different cellular properties relative to the FL RAG2 protein. Specifically, following genotoxic stress, there was no detectable nuclear export of the T490A RAG2 protein (18). Accordingly, RAG2 T490A showed an increased co-localization with H3K4me3-modified chromatin along with a significantly slower mobility than FL RAG2 in undamaged cells, which may contribute to its decreased export upon genotoxic stress (19). The recombination activity in the T490A-expressing stable clones was increased at the Igκ loci (in the absence or presence of STI-571) (Supl Fig 2). The increased recombination activity in STI-571-untreated cells for T490A versus FL RAG2 would be consistent with RAG-mediated DNA cleavage activity outside of G1 and its increased localization with chromatin. As shown with T490A knock-in mice (15), RAG-mediated DNA cleavage in other cell cycle phases may lead to aberrant DDR and DNA repair, with decreased cell recovery following the onset of genotoxic stress.

Altogether, our findings show RAG2 plays an important role in coordinating cellular responses to DNA damage by bolstering the DDR system. A robust DDR leads to the maintenance of cell viability in developing lymphocytes, which is critical for proper lymphocyte development. Improper regulation of RAG2 through disruption of either its cellular distribution or degradation can negatively affect cell recovery following exposure to DNA damaging agents.

Supplementary Material

Refer to Web version on PubMed Central for supplementary material.

Acknowledgements:

This work was supported by funds from the Oklahoma Center for Advancement in Science and Technology (HR18–072 to KR), the National Institutes of Health (AI128137 and AI156351 to KR; and T32AI007633 to WH), and the Presbyterian Health Foundation (to KR).

References

1. Gellert M (2002) V(D)J recombination: RAG proteins, repair factors, and regulation. Annu. Rev. Biochem. 71, 101–132 [PubMed: 12045092]
2. Schatz DG, and Ji Y (2011) Recombination centres and the orchestration of V(D)J recombination. Nat Rev Immunol 11, 251–263 [PubMed: 21394103]
3. Schatz DG, and Swanson PC (2011) V(D)J recombination: mechanisms of initiation. Annu Rev Genet 45, 167–202 [PubMed: 21854230]
4. Rodgers KK (2017) Riches in RAGs: Revealing the V(D)J Recombinase through High-Resolution Structures. Trends Biochem Sci 42, 72–84 [PubMed: 27825771]
5. Rooney S, Chaudhuri J, and Alt FW (2004) The role of the non-homologous end-joining pathway in lymphocyte development. Immunol Rev 200, 115–131 [PubMed: 15242400]
6. Lieber MR (2010) The mechanism of double-strand DNA break repair by the nonhomologous DNA end-joining pathway. Annu Rev Biochem 79, 181–211 [PubMed: 20192759]
7. Helmink BA, and Sleckman BP (2012) The response to and repair of RAG-mediated DNA double-strand breaks. Annu Rev Immunol 30, 175–202 [PubMed: 22224778]
8. Arya R, and Bassing CH (2017) V(D)J Recombination Exploits DNA Damage Responses to Promote Immunity. Trends Genet 33, 479–489 [PubMed: 28532625]
9. Bredemeyer AL, Sharma GG, Huang CY, Helmink BA, Walker LM, Khor KC, Nuskey B, Sullivan KE, Pandita TK, Bassing CH, and Sleckman BP (2006) ATM stabilizes DNA double-strand-break complexes during V(D)J recombination. Nature 442, 466–470 [PubMed: 16799570]
10. Meek K, Xu Y, Bailie C, Yu K, and Neal JA (2016) The ATM Kinase Restrains Joining of Both VDJ Signal and Coding Ends. J Immunol 197, 3165–3174 [PubMed: 27574300]
11. Bredemeyer AL, Helmink BA, Innes CL, Calderon B, McGinnis LM, Mahowald GK, Gapud EJ, Walker LM, Collins JB, Weaver BK, Mandik-Nayak L, Schreiber RD, Allen PM, May MJ, Paules RS, Bassing CH, and Sleckman BP (2008) DNA double-strand breaks activate a multi-functional genetic program in developing lymphocytes. Nature 456, 819–823 [PubMed: 18849970]
12. Innes CL, Hesse JE, Palii SS, Helmink BA, Holub AJ, Sleckman BP, and Paules RS (2013) DNA damage activates a complex transcriptional response in murine lymphocytes that includes both physiological and cancer-predisposition programs. BMC Genomics 14, 163 [PubMed: 23496831]
13. Villa A, and Notarangelo LD (2019) RAG gene defects at the verge of immunodeficiency and immune dysregulation. Immunol Rev 287, 73–90 [PubMed: 30565244]
14. Nambiar M, and Raghavan SC (2011) How does DNA break during chromosomal translocations? Nucleic Acids Res 39, 5813–5825 [PubMed: 21498543]
15. Zhang L, Reynolds TL, Shan X, and Desiderio S (2011) Coupling of V(D)J recombination to the cell cycle suppresses genomic instability and lymphoid tumorigenesis. Immunity 34, 163–174 [PubMed: 21349429]
16. Ochodnicka-Mackovicova K, Bahjat M, Maas C, van der Veen A, Bloedjes TA, de Bruin AM, van Andel H, Schrader CE, Hendriks RW, Verhoeyen E, Bende RJ, van Noesel CJ, and Guikema JE (2016) The DNA Damage Response Regulates RAG1/2 Expression in Pre-B Cells through ATM-FOXO1 Signaling. J Immunol 197, 2918–2929 [PubMed: 27559048]
17. Fisher MR, Rivera-Reyes A, Bloch NB, Schatz DG, and Bassing CH (2017) Immature Lymphocytes Inhibit Rag1 and Rag2 Transcription and V(D)J Recombination in Response to DNA Double-Strand Breaks. J Immunol 198, 2943–2956 [PubMed: 28213501]
18. Rodgers W, Byrum JN, Sapkota H, Rahman NS, Cail RC, Zhao S, Schatz DG, and Rodgers KK (2015) Spatio-temporal regulation of RAG2 following genotoxic stress. DNA Repair (Amst) 27, 19–27 [PubMed: 25625798]
19. Rodgers W, Byrum JN, Simpson DA, Hoolehan W, and Rodgers KK (2019) RAG2 localization and dynamics in the pre-B cell nucleus. PLoS One 14, e0216137 [PubMed: 31075127]
20. Jiang H, Chang FC, Ross AE, Lee J, Nakayama K, and Desiderio S (2005) Ubiquitylation of RAG-2 by Skp2-SCF links destruction of the V(D)J recombinase to the cell cycle. Mol Cell 18, 699–709 [PubMed: 15949444]

21. Jackson SP, and Bartek J (2009) The DNA-damage response in human biology and disease. Nature 461, 1071–1078 [PubMed: 19847258]

22. Wang F, and Higgins JM (2013) Histone modifications and mitosis: countermarks, landmarks, and bookmarks. Trends Cell Biol 23, 175–184 [PubMed: 23246430]

23. Deriano L, Chaumeil J, Coussens M, Multani A, Chou Y, Alekseyenko AV, Chang S, Skok JA, and Roth DB (2011) The RAG2 C terminus suppresses genomic instability and lymphomagenesis. Nature 471, 119–123 [PubMed: 21368836]

24. Raval P, Kriatchko AN, Kumar S, and Swanson PC (2008) Evidence for Ku70/Ku80 association with full-length RAG1. Nucleic Acids Res 36, 2060–2072 [PubMed: 18281312]

25. Shimada M, and Komatsu K (2009) Emerging connection between centrosome and DNA repair machinery. J Radiat Res 50, 295–301 [PubMed: 19542690]

26. Karo JM, Schatz DG, and Sun JC (2014) The RAG Recombinase Dictates Functional Heterogeneity and Cellular Fitness in Natural Killer Cells. Cell 159, 94–107 [PubMed: 25259923]

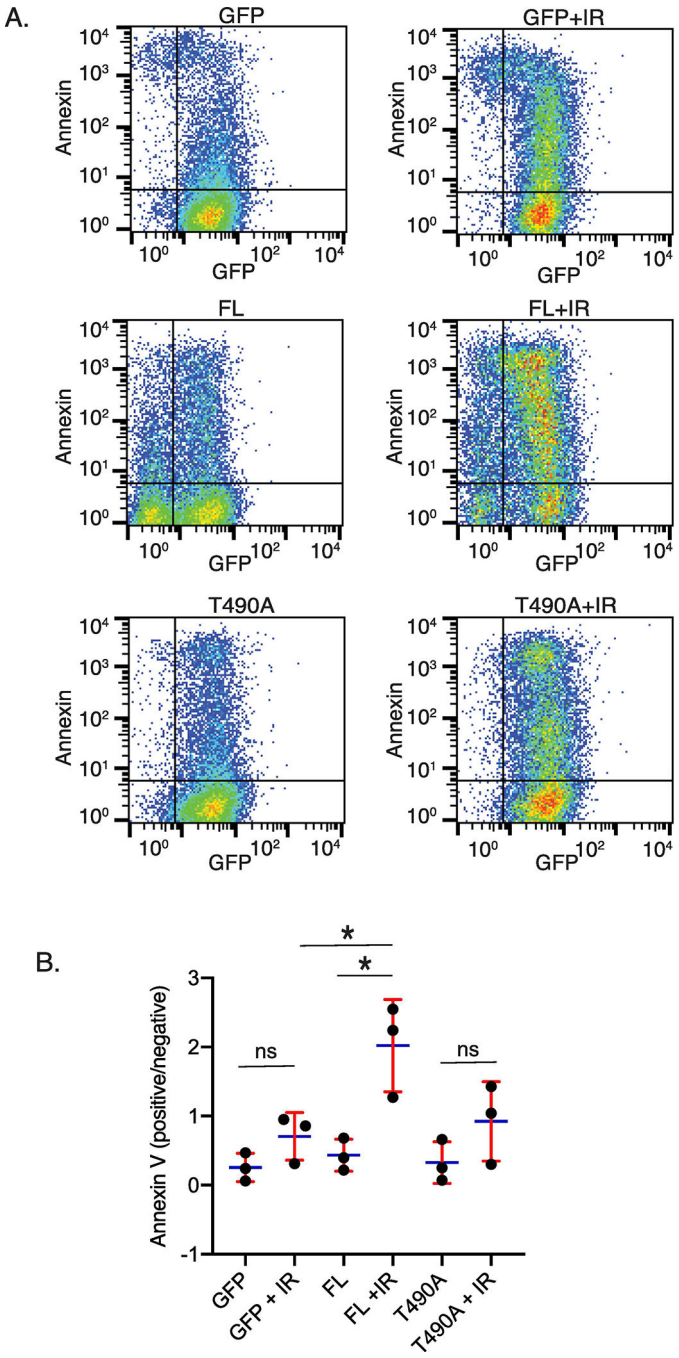

Figure 1. FL RAG2-expressing cells show a higher burst of apoptosis following IR as compared to T490A and GFP control-expressing cells.

(A) Flow cytometry measuring GFP fluorescence in cells that expressed GFP alone, or GFP fused to FL or T490A RAG2. Measurements were made before and 24 hrs following IR. Plots are representative of 3 separate trials (Annexin, Annexin V) **(B)** Averaged ratios of Annexin V positive to negative cells for each sample. Error bars represent SD, n=3. *, $p<0.05$ by student's *t* test; ns, not significant

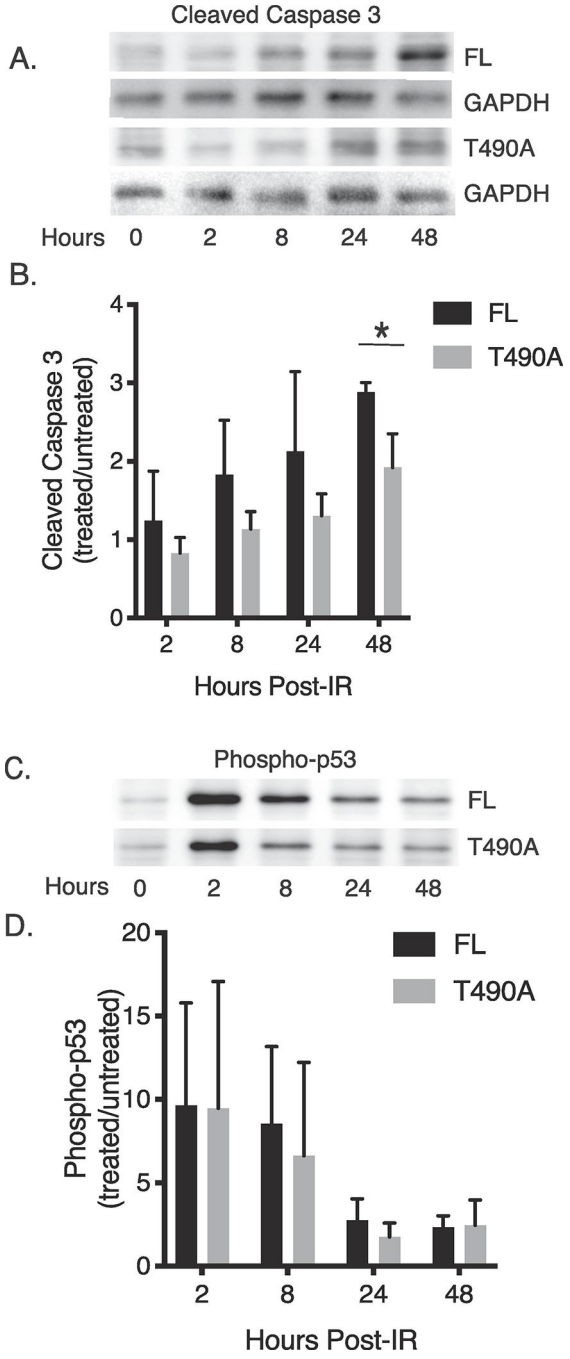

Figure 2. IR-induced effects on levels of cleaved caspase-3 and phosphorylated p53 in RAG2-expressing cells.

(A) Detection of caspase-3 cleavage in cells that expressed either FL or T490A. The samples were prepared at the indicated times following IR. In **(B)** is plotted the averaged ratio of caspase-3 cleavage measured in treated and untreated samples at each time point. The error bars represent SD (n=3). **(C)** Detection of p53 phosphorylation following IR in cells that expressed either FL or T490A. In **(D)** is the averaged ratio of p53 phosphorylation in treated

and untreated cells measured at the indicated time points following IR. The error bars represent SD (n=3). *, $p<0.05$ by student's *t* test

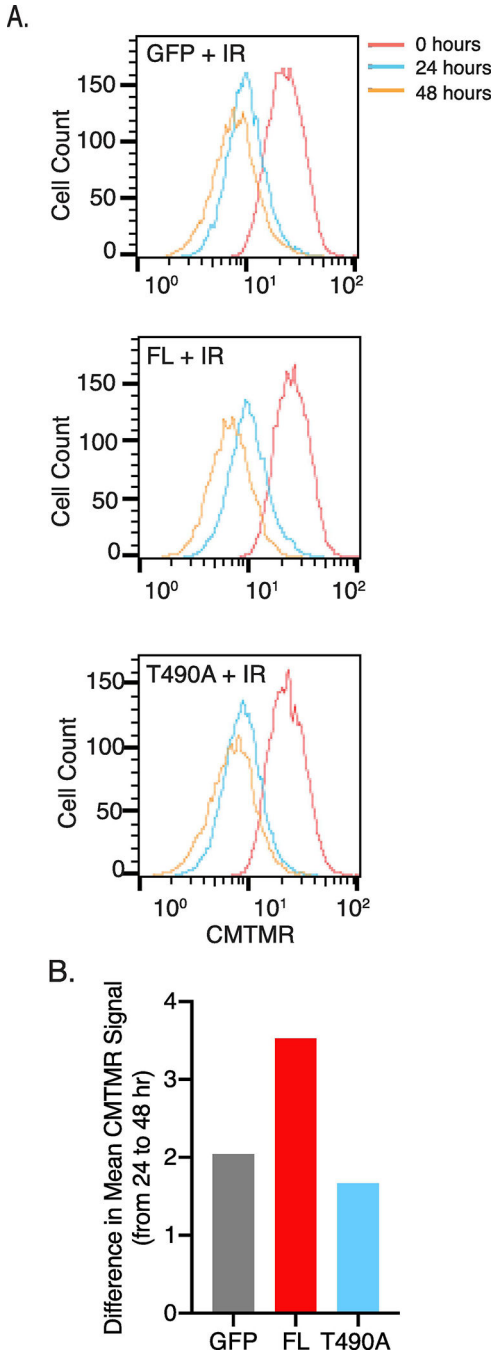

Figure 3. FL RAG2-expressing pre-B cells show increased pre-B cell proliferation after 24 hrs post-IR.

(A) Cell proliferation analysis using flow cytometry. Proliferation was measured by the decrease in Cell Tracker Orange (CMTMR) label due to cell division. Samples were treated with IR, labeled with CMTMR, and then returned to culture for the indicated times before flow cytometry. In **(B)** is the difference in peak mean fluorescence intensity between 24 and 48 hrs following IR for each sample. The data are a representative example of 3 separate trials.

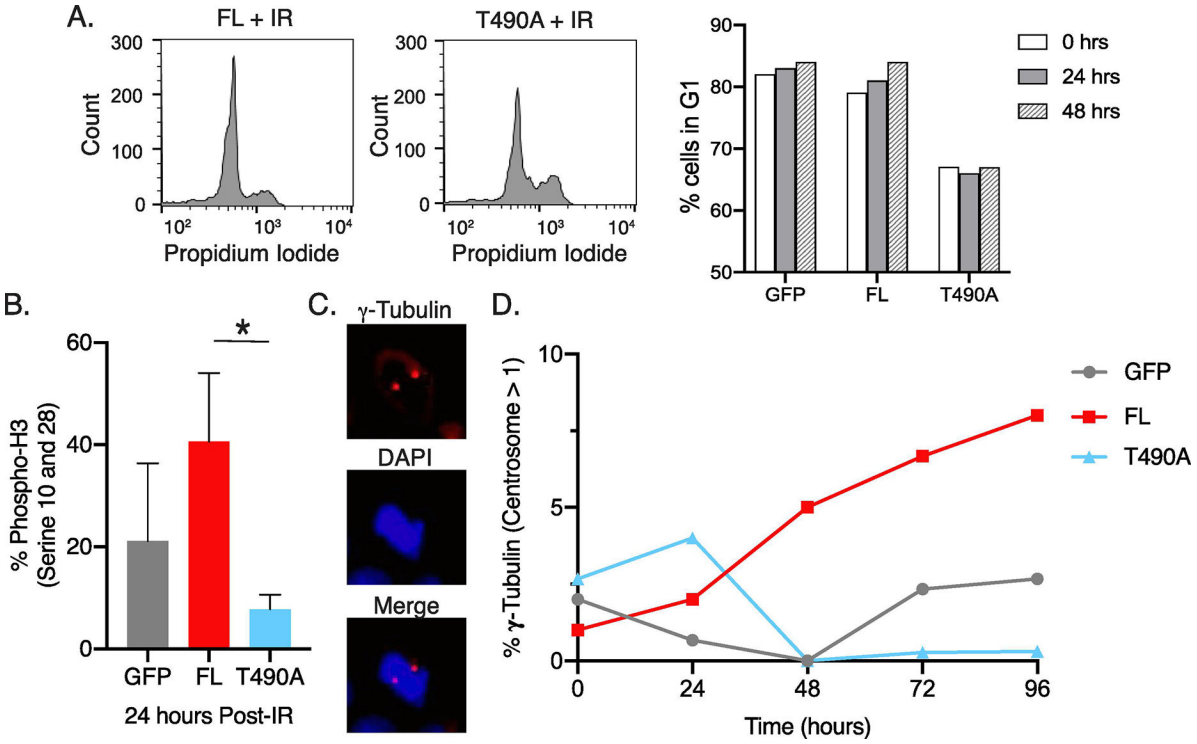

Figure 4. Elevation in markers for mitosis following IR in pre-B cells expressing FL RAG2.

(A) Representative flow cytometry plots of propidium iodide stained FL and T490A clones 24 hrs post-IR, indicating cell cycle phases (left flow plots). Representative plots of % FL, T490A, and GFP control cells in the G1 cell cycle phase at the indicated timepoints post-IR. **(B)** Detection of histone 3 (H3) phosphorylation at Ser10, Ser28, and Thr11. At 24 hr post-IR, cells were immunostained with antibody to phospho-H3, and then measured by flow cytometry. Error bars represent SD (n=3). *, $p<0.05$ by student's *t* test **(C)** Representative microscope images of pre-B cells that expressed FL cells and stained with antibody to gamma-tubulin and secondary antibody DyLight 594 (top) and DAPI (middle) 24 hrs following IR. The bottom image is a merge of the gamma-tubulin and DAPI stains. **(D)** Quantification of gamma-tubulin stain for each sample at indicated times following IR. Centrosome numbers per cell were determined from at least 20 different cells per sample and the values plotted versus timepoints post-IR. The data are a representative example of 3 separate trials.

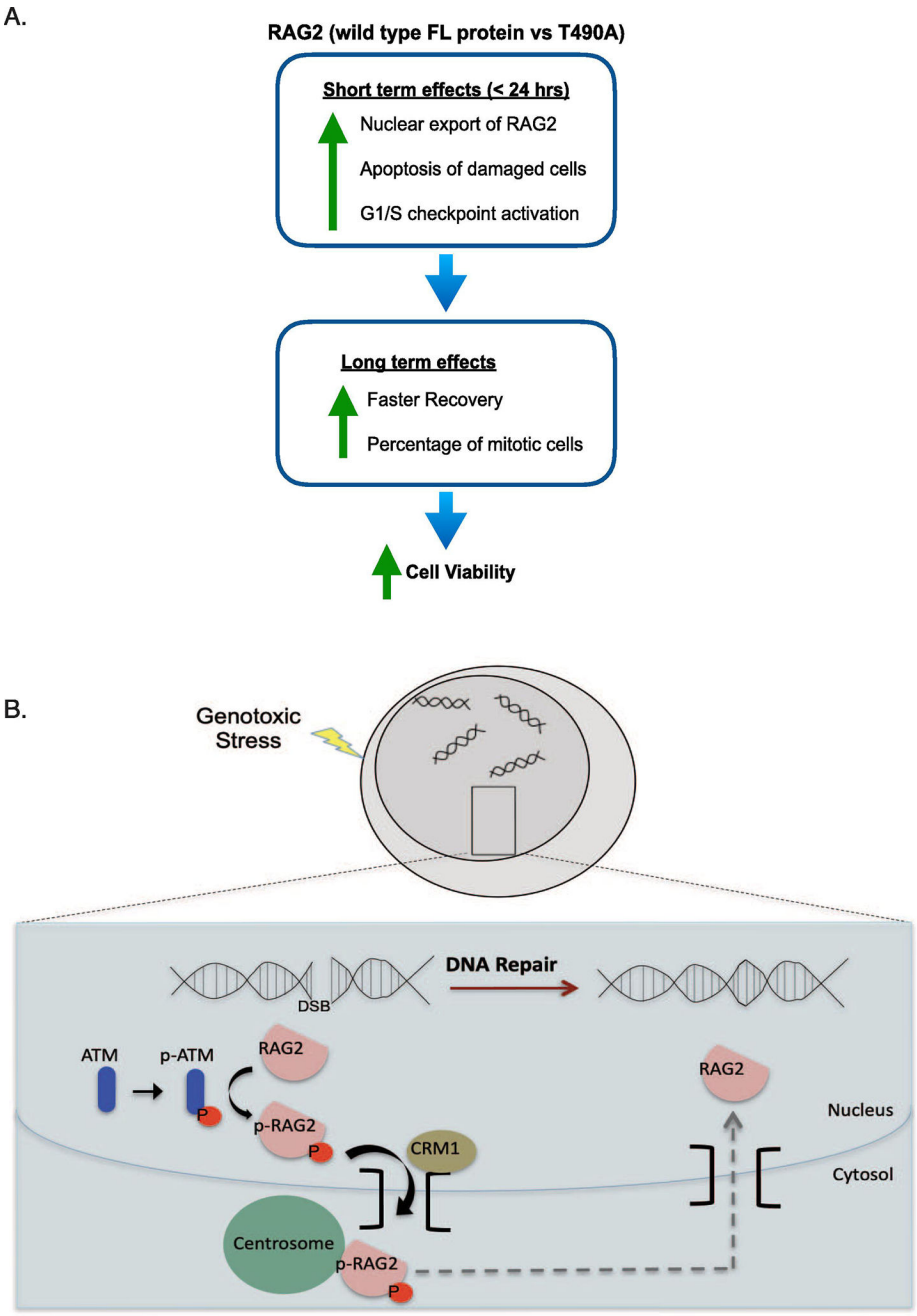

Figure 5. Model for the effect of FL RAG2 on the DDR in developing B cells.

(A) In the short term (within 24 hrs post-IR), RAG2 exports from the nucleus, followed by levels of robust apoptosis and checkpoint activation. After the initial burst in apoptosis of damaged cells, RAG2-expressing cells show an increased growth rate and an increased percentage of mitotic cells. Altogether, the FL-expressing cells demonstrate increased cell viability following genotoxic stress relative to either the T490A-expressing or GFP control-expressing cells. **(B)** Model for nuclear export of FL RAG2 upon genotoxic stress. RAG2 includes core and non-core (nc) regions. The nc region mediates both nuclear export and centrosome targeting, as core RAG2 does not localize to the centrosome following DNA

damage, and mutation of threonine 490 (T490) to alanine blocks nuclear export of full length RAG2 (18). Nuclear export of RAG2 is dependent on ATM and exportin-1/CRM1.